Open Access

Advances in Environmental and Engineering Research

LIDSEN Publishing Inc.

Research Article

Photodegradation of Polyethersulfone (PES), Polyvinylidene Fluoride (PVDF) and Polymethyl Methacrylate (PMMA) Microplastics via a Metal Organic Framework Namely ZIF-8/ZnO/C

Rukiye Öztekin, Delia Teresa Sponza *

Department of Environmental Engineering, Engineering Faculty, Dokuz Eylül University, Tınaztepe Campus, 35160 Buca/İzmir, Turkey; E-Mails: rukiyeoztekin@gmail.com; delya.sponza@deu.edu.tr

* **Correspondence:** Delia Teresa Sponza; E-Mail: delya.sponza@deu.edu.tr

Academic Editor: Islam Md Rizwanul Fattah

Special Issue: Advances in Environmental Research

Adv Environ Eng Res
2024, volume 5, issue 4
doi:10.21926/aeer.2404019

Received: August 27, 2024
Accepted: October 08, 2024
Published: October 17, 2024

Abstract

The aim of this study was to photodegrade the Polyethersulfone (PES), Polyvinylidene fluoride (PVDF) and Polymethyl methacrylate (PMMA) microplastics using Zeolitic imidazolate framework-8/Zinc oxide/Carbon (ZIF-8/ZnO/C) nanocomposite generated under laboratory conditions. The produced nanocomposite was analysed using X-Ray Diffraction (XRD), Fourier Transform Infrared Spectroscopy (FTIR), X-Ray Photo Spectroscopy (XPS), Scanning Electron Microscope (SEM), Diffuse reflectance UV-vis spectra (DRS) and Electron Spin Resonance (ESR) analyses. The maximum PES, PVDF and PPMA photodegradation yields were 99%, 98%, and 96%, respectively, at 1 mg/l ZIF-8/ZnO/C nanocomposites (NCs) concentration, 1000 mg/l microplastics concentration, at pH = 10.0, at a temperature and photodegradation time of 40°C and 20 min, under oxic conditions at a sunlight intensity of 80 W/m^2 and a photon yield of 16. The XRD analysis showed the generation of ZIF-8/ZnO/C, while the FTIR analysis indicated the ZnO, C, and ZIF-8.

Keywords
Photodegradation; polyethersulfone (PES); polyvinylidene fluoride (PVDF); polymethyl methacrylate (PPMA); metal organic framework (MOF); microplastics; zeolitic imidazolate framework-8/zinc oxide/carbon (ZIF-8/ZnO/C)

1. Introduction

Microplastics have small structures and are smaller than 5 mm in size. They are not biologically degradable and can be easily transformed in the environment. The concentrations of microplastics are highly increased in the sea, soil environments, food, and tap water. Microplastics have accumulated since and were not easily biodegraded in the ecosystem. Among these microplastics polyethersulfone (PES) has an amorphous shape and is resistant to high temperatures. Therefore, it is commercially present in PES plastic resins and exhibits high resistance. PES exhibited high absorptions and can be used to make the solvents. Polysulfones are relevant to a family that exhibits high performance in thermoplastics. These PES exhibited toughness and stability properties at elevated temperatures. Commercial polysulfones have an aryl-SO_2-aryl group. Due to the high cost, polysulfones are used in the production of polycarbonates. Three polysulfones are present: polysulfone (PSU), polyethersulfone (PES/PESU), and polyphenylene sulfone (PPSU). They are used at high temperatures like between -100°C and +200°C. They are used in electrical installations, car production, and medical applications [1]. They are composed of aromatics, sulfonyl ether, and alkyl groups. Polysulfones are resistant to hydrolysis and alkaline environments and have good electrical properties. The chemical structure of PES is shown in Figure 1.

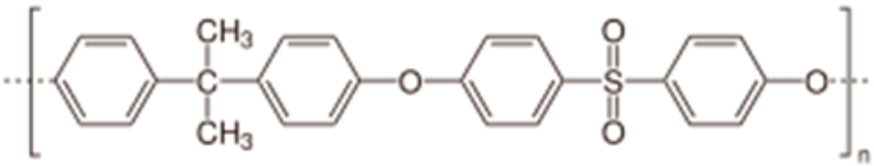

Figure 1 Chemical structure of PES.

Polyvinylidene difluoride (PVDF) is resistant to reactions and was produced from vinylidene difluoride's polymerization [1]. Its chemical formula is $(C_2H_2F_2)_n$. PVDF is extensively used in microplastic applications and is resistant to solvents, acids, and hydrocarbons. PVDF density is low (1.78 g/cm^3) compared to polytetrafluoroethylene (PTFE). It is used in the piping instruments, tubing, films, and plates. It can be used in chemical, semiconductor, medical, and defense industries. It is also used in foam production and exhibits 3D filament properties [1]. The chemical properties of PVDF are shown in Figure 2.

Figure 2 Chemical properties of PDVF.

Poly (methyl methacrylate) (PMMA) is produced from methyl methacrylate [1]. It is used as an engineering plastic with transparent properties. PMMA is also known as acrylic, Lucite, and Perspex, among several others. This plastic is used as a shatter-resistant alternative to glass. It can also be used as a casting resin and coatings [1]. The chemical properties of PMMA are shown in Figure 3.

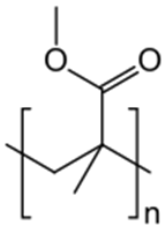

Figure 3 Chemical properties of PMMA.

The recent studies performed by photodegradation of some microplastics, namely polyethylene (PE), polypropylene (PP), Polyvinyl chloride (PVC), and carbon fiber (SCF) filled ethylene methyl acrylate (EMA), Polyvinylidene difluoride (PVDF) and Poly (methyl methacrylate) (PMMA) with different nanocomposites were summarized as follows:

Ding et al. [2] investigated the removal of polyethylene (PE) and polypropylene (PP) microplastics as emerging contaminants in textile dyeing sludge (TDS). Microplastics' presence and types inevitably influence TDS's combustion and pyrolysis. Their effects on the co-combustion/pyrolysis emissions and residual metals of TDS remain poorly understood. Their study aimed to quantify the impacts of polyethylene (PE) and polypropylene (PP) on the transports and transformations of gaseous emissions and residual metals generated during TDS combustion and pyrolysis in the air, oxy-fuel, and nitrogen gas N_2(g) atmospheres [2]. Thermal degradation of microplastics in TDS occurred between 242-600°C. TDS played a significant role in promoting the initial release of plastic volatiles [2]. Microplastics were increased by releasing volatile organic carbons (VOCs), and the types of VOCs under the combustion and pyrolysis conditions and non-oxygenated organics and hydrocarbons were released into the environment [2]. Liu et al. [3] aimed to characterize gas products and bottom slag of the catalytic pyrolysis of medical waste infusion of Polyvinyl chloride and PVC tubes using $FeAlO_x$ as a bimetallic catalyst to turn the carbon (C) into CO [3]. With $FeAlO_x$ catalyst, the C-Cl bond in PVC degraded, increasing hydrochloric acid (HCl) and light hydrocarbon gas emissions (e.g., methane, CH_4) [3]. The addition of $FeAlO_x$ increased energy consumption and caused an increase in pollutant emissions.

Das et al. [4] presented a synthesis of extensive research on using 2 dimensional (2D) materials for removing microplastics. This material consists of graphene, graphene oxide, and transition metal dichalcogenides and can be used in the PMMA microplastics remediation procedures [4]. Das et al. [5] used polymer nanocomposites (PNCs) to remove the PP microplastics using catalytic and redox degradation processes. Das [6] researched the application of polymer composites in various sensor devices to remove the PVDF microplastics [6]. Bhawal et al. [7] researched the short carbon fiber (SCF) filled ethylene methyl acrylate (EMA) NCs to remove the PP microplastics.

According to the photocatalytic research given above for removing the microplastic, namely, PP, PE, and PMMA, low removal yields were detected, some ultimate gases and products negatively affect the environment, and the treatment costs are incredibly high. Therefore, it is necessary to produce economical and eco-friendly procedures to clean the pollutants in wastewater [8-10]. In

recent years, ZnO has been extensively used during the photodegradation of organics because of its non-toxic, low cost, and high photodegradation yield [11-14]. On the other hand, ZnO has a wide band gap and low specific surface area. To overcome this problem, some procedures, such as formation doping and non-doping metals, and some organics have large surface areas [15]. Metal-organic frameworks (MOFs) are porous materials with metal oxides and rigid or semi-rigid organic connections. MOFs have been extensively used in recent years due to their large surface area [16]. Zinc-based MOFs exhibited high performance in the photodegradation of organic pollutants with metal sites [17]. ZIF-8 MOFs exhibited high chemical and thermal stability compared to other MOF groups. However, the recombination of excited electron holes decreases the photodegradation yields. Combining ZIF-8 with appropriate carbon groups reduces the redox efficiency of electron carriers and increases the photodegradation efficiency.

In comparison with other photo nanocomposites, MOF nanocomposites have excellent advantages. i) High surface area and high porosity provide rapid mass transfer and, as a result, photocatalytic points accelerate the substrate's transport. ii) the structures provide great light absorption surfaces. Therefore, many scientists generate various MOFs with macroporous and single crystalline structures composites as photonanocomposites, improving the molecular mass transfer yields [18, 19].

Among all the metal oxide electrodes, ZnO is exceptional due to its low cost, chemical durability, and high energy efficiency [20]. ZnO nanoparticles on the surroundings of ZIF-8 can extensively control the surfaces and interfacial places and then generate the heterostructure. The macroporous structure improved carrier mobility, mass transfer efficiency, and light utilization during photocatalysis. On the other hand, carbon has been widely used due to its high electrical conductivity, large surface area, and good thermal/chemical durability [21]. The yield can improve by generating a composite using ZnO and carbon. By spying on ZnO surrounding carbon, the generating composite showed a high photocatalytic activity [22]. This is because carbon regulates active sites at the surfaces, has high chemical durability, and can transfer twice higher values of yield [23]. Adding an external carbon source to the ZnO/C composite can elevate their charge storage capacity with ZIF-8, ending with higher efficiency and long durability.

The studies performed by ZIF-8 MOF containing ZnO were summarized as follows: Ding et al. [24] investigated the photocatalytic yields of ZIF-8/ZnO/Ca degrading organic compounds. Liu et al. [13] investigated the ZIF-8 MOF-derived carbon modified with ZnO photocatalysts to improve the photocatalytic CO_2 removal. He et al. [25] fabricated the ZnO nanoparticles derived from ZIF-8 MOF with visible light for photocatalytic hydrogen production. Abdollahi et al. [26] researched the photoremoval of dyes by ZIF-8 metal organic framework (MOFs)-based CuO-ZnO photocatalyst under solar irradiation. Chao et al. [27] investigated the removal of tetracycline. Antibiotic with modified ZIF-8 fibers. Pasanen et al. [28] prepared a ZIF-8 magnetic porous nanocomposite (nano-Fe@ZIF-8) to remove the microplastics and plastic-derived endocrine disruptors.

The recent studies summarized above investigated the degradation of microplastics, namely polyvinyl chloride carbon filters containing polyvinyl microplastics such as polyethylene and polypropylene. No data on PES, PVDF, and PMMA microplastics photodegradation was found. No study was detected for photo removal of the aforementioned microplastics with C, ZnO, ZIF-8, and ZIF-8/ZnO/C NCs. Furthermore, the quantum yield and band gap energies of C, ZnO, ZIF-8 and ZIF-8/ZnO/C NCs were not measured yet.

As mentioned, a lot of pollutants were removed by the ZnO nanoparticles derived from ZIF-8. Until now, only two studies have investigated the photo removals of PES, PVDF, and PMMA microplastics by ZIF-8.

Therefore, in this study in order to photoremoval of microplastics namely, PES, PVDF and PMMA microplastics, a MOF nanocomposite, namely, ZIF-8/ZnO/C was produced under laboratory conditions. The produced nanocomposite and C, ZnO, ZIF-8 were analysed using XRD, FTIR, XPS, SEM, DRS and ESR analyses. The effects of increasing ZIF-8/ZnO/C NCs concentrations (0.1-3 mg/l), photodegradation time (10-80 min), increasing concentrations of PES, PVDF and PMMA (100-1200 mg/l), pH (5.0, 7.0 and 10.0), sunligth power (20-120 W/m^2) and temperature (20-40°C) on the photodegradation yields of PES, PVDF and PMMA microplastics were investigated. Furthermore, the quantum yield and band gap energies of C, ZnO, ZIF-8 and ZIF-8/ZnO/C NCs were compared.

2. Materials and Methods

2.1 Materials

Acetone, ethyl alcohol, methyl alcohol, glucose, zinc acetate ($Zn(CH_3COO)_2$), ammonium hydroxide (NH_4OH), and zinc nitrate ($Zn(NO_3)_2$) were purchased from Merck (Germany) and without further purification. 2-Methylimidazole was obtained from Sigma-Aldrich (Germany). Carbon (C), Polyethersulfone (PES), Polyvinylidene fluoride (PVDF), and Polymethyl methacrylate (PMMA) microplastics were purchased from Merck (Germany).

2.2 Synthesis of Photocatalytic Materials

The ZIF-8/ZnO/C NCs was generated as follows: 10 g raw carbon was mixed with 80 ml acetone, ethyl alcohol, and 40 ml deionized water for 20 h at 23°C room temperature. Then, the carbon was prepared by washing and drying at 90°C for 3 h. Then, activated carbon was get by hydrothermal procedure with 40 g/l glucose. This reaction was performed in a 200 ml reactor at 250°C for 3 h. The carbon was washed with deionized water and dried at 90°C. Then, 400 ml solution was prepared with 9.50 g $Zn(CH_3COO)_2$ and 5 g NH_4OH for 40 h at 30°C. As a result, ZnO-Carbon was detected after drying at 90°C for 2 h. 3.90 g of $Zn(NO_3)_2$ was added to 120 g methyl alcohol for 40 min. 7.90 g of 2-methylimidazole was dissolved in 250 ml methyl alcohol. ZnO-Carbon was put into the 2-methylimidazole solution for 20 min, and $Zn(NO_3)_2$ solution was prepared by mixing for 18 h at 80°C. The ZIF-8/ZnO/C was generated after washing and drying procedures.

2.3 Photodegradation Measurements

The ultraviolet (UV) irradiation treatments were performed using sun light at different time intervals (morning 8.00 am, 10.00 am, 12.00 am, 13.00 pm, 15.00 pm, 16.00 pm, 17.00 pm in August) to adjust the intensity a W/m^2. At given different photodegradation time intervals, the suspension of 10 ml was sampled and separated by centrifuge, then analyzed according to the absorbance between λ_{max} = 200 nm and λ_{max} = 500 nm by a UV-vis spectrometer (Cary 5000 UV-Vis Spectrophotometer from Varian, Siemens, Germany) with a Quartz cuvette.

2.4 Characterization

XRD analysis was performed on a Shimadzu XRD-7000, Japan diffractometer using Cu Kα radiation (λ = 1.6000 Å, 50 kV, 50 mA) at a scanning velocity of 1.7°/min in the 13-85° 2θ range. Raman spectrum was detected with a Horiba Jobin Yvon-Labram HR UV-Visible NIR (200-1600 nm) Raman microscope spectrometer at 520 nm. The Raman spectrum was achieved from 12 scans at a resolution of 2.4/cm. The FTIR spectra were measured using the FT-NIR spectroscope (RAYLEIGH, WQF-510). ZIF-8/ZnO/C samples were scanned using infrared light, and their chemical properties were obtained using FTIR spectra. The samples' valence state was investigated and analyzed using XPS (ESCALAB 250Xi, England). With Al Kα source surface, chemical composition and reduction state analyses were performed at 35 eV. The peak of disturbances was done using XPS-peak 41 software. SEM (FESEM, Hitachi S-4700) investigated the generated catalyst's morphological properties. SEM investigated the composition of the elements in the ZIF-8/ZnO/C. Diffuse reflectance UV-vis spectra (DRS) between 200 and 800 nm were recorded on a Varian 5000 spectrophotometer.

2.5 Quantum Yield During Photodegradation

Both hydroxyl and superoxide radicals ($OH^{\bullet}$ and $O_2^{-\bullet}$) were produced from nanocomposites during photodegradation under UV, which was investigated by the measurements of the intensity of active species performed by the electron spin resonance (ESR). Compared with ZnO/C and ZIF-8/C, ZIF-8/ZnO/C NCs showed a more substantial peak disturbance with characteristic peaks of $OH^{\bullet}$ and $O_2^{-\bullet}$ during photodegradation. In the photocatalytic process, the production of $O_2^{-\bullet}$ can be defined with the reaction between electrons and surface adsorbing the oxygen, while $OH^{\bullet}$ indicates the holes re-reacting with $OH^{-\bullet}$. The presence of $O_2^{-\bullet}$ contributes to the yield of $OH^{\bullet}$. The organics can be photodegraded by $OH^{\bullet}$ and $O_2^{-\bullet}$ in redox [29]. The time-dependent differential quotient calculated the quantum yield according to Eq. 1 [30].

$$\Phi_{diff}(t) = \frac{\Delta N_{product}(t)}{\Delta N_{photon}(t)} \quad (1)$$

Where Δ*N* was the increase in substrate over a time interval Δ*t* and Δ*N* photon exhibits the number of absorbed photons during that t time.

2.6 Microplastic Measurements

The microplastics studied in this study was measured according to the method developed by Dong et al. [31].

2.7 Statistical Analysis

Regression analysis between variables was performed using the EXCELL in Microsoft WindowsTM (HP, USA). The linear correlation was assessed with r^2. The r^2 value is the correlation coefficient and reflects statistical significance between dependent and independent variables. Analysis of variance (ANOVA) (SAS ANOVA procedure) test was used to assess the data obtained in reactors using the EXCELL in Microsoft WindowsTM (HP, USA).

3. Results and Discussions

3.1 XRD Analysis Results

The results of XRD analysis were obtained after the photodegradation process for PES, PVDF, and PMMA microplastics with ZIF-8/ZnO/C NCs (Figure 4). The characterization peaks of C were found at 2θ values of 5.64°, 11.17°, 14.36°, 15.45°, 17.25°, 18.58°, 19.12°, 23.24°, 24.71°, 27.26°, 28.52°, 30.20°, 31.02°, 32.68°, 33.75°, 34.77°, 35.49°, 37.41° and 43.08°, respectively, and which can also be indexed as (101), (210), (204), (110), (201), (312), (220), (012), (111), (100), (210), (213), (112), (301), (103), (102), (013), (203) and (212), respectively (Figure 4, black pattern). The characterization peaks of ZnO were observed at 2θ values of 5.68°, 10.54°, 14.42°, 18.31°, 23.39°, 27.45°, 34.71° and 37.89°, respectively, and which can also be indexed as (210), (110), (201), (220), (111), (102), (012) and (113), respectively (Figure 4, red pattern). The characterization peaks of ZIF-8 were obtained at 2θ values of 5.70°, 10.50°, 13.48°, 18.63°, 25.87°, 27.11°, and 33.49°, respectively, and which can also be indexed as (110), (211), (120), (101), (122), (022) and (100), respectively (Figure 4, green pattern). The characterization peaks of ZIF-8/ZnO/C NCs were measured at 2θ values of 5.52°, 10.15°, 14.32°, 18.10°, 28.14°, 32.01° and 34.47°, respectively, and which can also be indexed as (121), (010), (120), (020), (101), (202) and (111), respectively (Figure 4, purple pattern). This phenomenon indicated that the nucleation site was formed, which can be explained as "the mold can provide metal oxide by sacrificing the self-released metal ions".

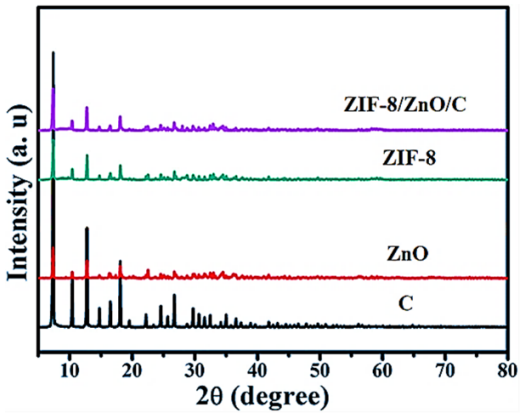

Figure 4 XRD pattern of C (black pattern), ZnO (red pattern), ZIF-8 (green pattern) and ZIF-8/ZnO/C NCs (purple pattern), after photodegradtion process for PES, PVDF and PMMA microplastics with ZIF-8/ZnO/C NCs, respectively.

3.2 FTIR Analysis Results

The FTIR spectrum of ZnO, C, ZIF-8, and ZIF-8/ZnO/C NCs was determined after the photodegradation process for PES, PVDF, and PMMA microplastics with ZIF-8/ZnO/C NCs (Figure 5). The maximum disturbances for ZnO in the FTIR spectra were detected at 3500 cm^{-1}, 2350 cm^{-1}, 1400 cm^{-1}, 850 cm^{-1}, 550 cm^{-1}, and 500 cm^{-1} wavenumbers, respectively (Figure 5, black spectra). The maximum disturbances for C in FTIR spectra were detected at 3450 cm^{-1}, 3250 cm^{-1}, 2850 cm^{-1}, 1600 cm^{-1}, 1400 cm^{-1}, 1350 cm^{-1}, 1280 cm^{-1}, 1180 cm^{-1}, 1150 cm^{-1}, 1000 cm^{-1}, 750 cm^{-1}, 600 cm^{-1}, 530 cm^{-1} and 375 cm^{-1} wavenumbers, respectively (Figure 5, blue spectra). The maximum disturbances of FTIR spectrum for ZIF-8 were observed at 3125 cm^{-1}, 2850 cm^{-1}, 2200 cm^{-1}, 1600 cm^{-1}, 1490 cm^{-1},

1350 cm^{-1}, 1300 cm^{-1}, 1200 cm^{-1}, 1150 cm^{-1}, 1000 cm^{-1}, 750 cm^{-1}, 600 cm^{-1}, 575 cm^{-1} and 480 cm^{-1}, wavenumbers, respectively (Figure 5, green spectra). The maximum disturbances of ZIF-8/ZnO/C NCs in FTIR spectra were illustrated at 3130 cm^{-1}, 2930 cm^{-1}, 2400 cm^{-1}, 1580 cm^{-1}, 1425 cm^{-1}, 1300 cm^{-1}, 1250 cm^{-1}, 1200 cm^{-1}, 1000 cm^{-1}, 750 cm^{-1}, 700 cm^{-1} and 450 cm^{-1} wavenumbers, respectively (Figure 5, yellow spectra).

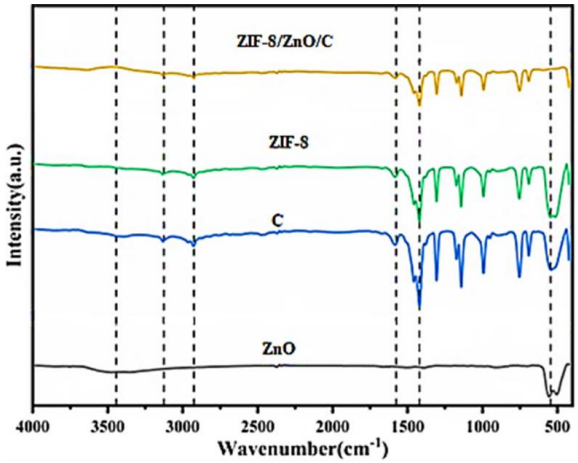

Figure 5 FTIR spectrum of ZnO (black pattern), C (blue pattern), ZIF-8 (green pattern), and ZIF-8/ZnO/C MOF (yellow pattern) after photodegradation process for PES, PVDF and PMMA microplastics with ZIF-8/ZnO/C NCs.

3.3 XPS Analysis Results

The XPS analysis of C, ZnO, ZIF-8 and ZIF-8/ZnO/C NCs were performed to investigate the photodegradation process for PES, PVDF and PMMA microplastics with ZIF-8/ZnO/C NCs (Figure 6). The maximum absorbance were detected at binding energies of 1208.12 eV, 1150.08 eV, 400.05 eV, and 290.59 eV for ZIF-8/ZnO/C NCs (Figure 6, purple spectra), 1309.63 eV, 1150.14 eV, 550.58 eV, and 285.74 eV for ZIF-8 (Figure 6, green spectra), 1308.36 eV, 1125.11 eV, 552.18 eV, 500.03 eV and 183.45 eV for ZnO (Figure 6, blue spectra), and 550.71 eV, and 290.81 eV for C (Figure 6, red spectra), respectively, after photodegradation process for PES, PVDF and PMMA microplastics with ZIF-8/ZnO/C NCs.

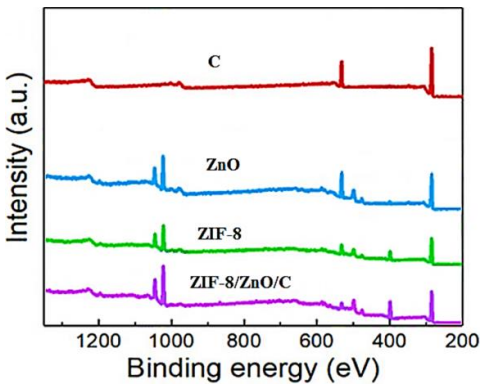

Figure 6 XPS spectrum of ZIF-8/ZnO/C NCs (purple spectra), ZIF-8 (green spectra), ZnO (blue spectra) and C (red spectra) after the photodegradation process for PES, PVDF, and PMMA microplastics with ZIF-8/ZnO/C NCs.

3.4 SEM Analysis Results

The morphological features of ZIF-8/ZnO/C NCs were characterized through SEM images after photodegradation for PES, PVDF, and PMMA microplastics with ZIF-8/ZnO/C NCs (Figure 7).

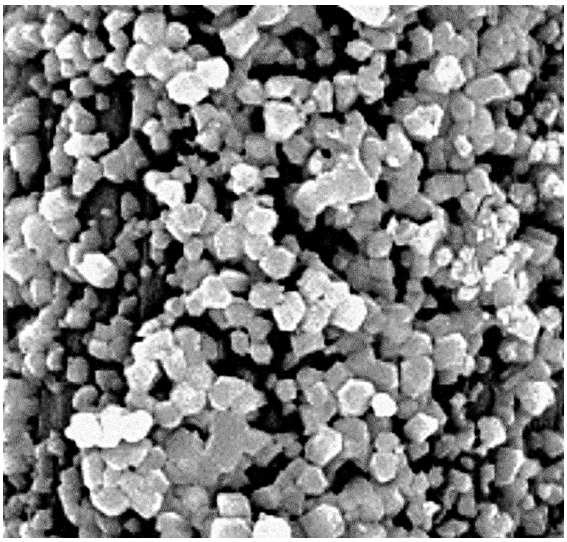

Figure 7 SEM images of ZIF-8/ZnO/C NCs after the photodegradation process for PES, PVDF and PMMA microplastics with ZIF-8/ZnO/C NCs (FESEM image size: 5 μm).

3.5 DRS Analysis Results

In the comparison of C (Figure 8, purple curve), ZnO (Figure 8, blue curve) and ZIF-8 (Figure 8, green curve) it was detected a very high electron absorption in the UV region at 240 nm, 275 nm and 250 nm, respectively. On the other hand, the band gap energies of C, ZnO and ZIF-8 were detected as 3.20 eV, 3.48 eV, and 3.25 eV, respectively.

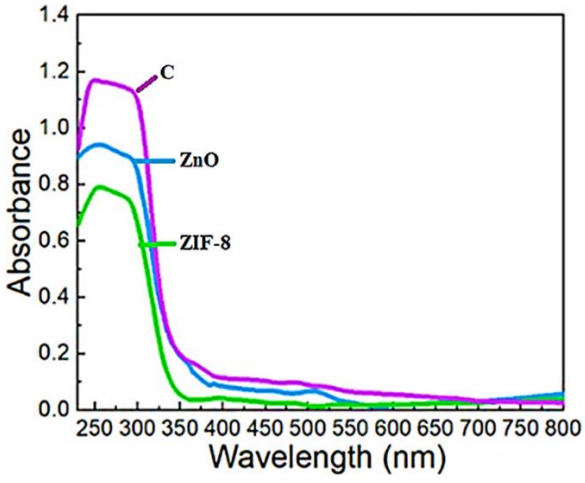

Figure 8 DRS curves of C (purple curve), ZnO (blue curve) and ZIF-8 (green curve), respectively.

3.6 ESR Analysis Results

Figure 9 exhibited the intensity of all activated species detected by electron spin resonance under UV photodegradation for $OH^{\bullet}$ and $O_2^{-\bullet}$ generated during photo-oxidation. For ZIF-8 (Figure 9, green spectra), ZnO (Figure 9, blue spectra), and C (Figure 9, purple spectra), it was observed that the spectra generally concentrated with higher values in the magnetic field between 3480 G and 3530 G. The data obtained exhibited that the activated types generated during photodegradatiın were O_2^-, H^+, and $OH^{\bullet}$.

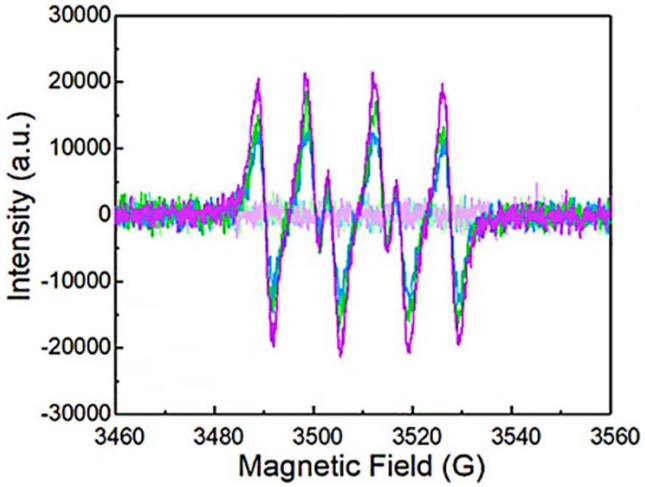

Figure 9 ESR spectrum of ZIF-8 (Green spectra), ZnO (Blue spectra), and Carbon (Purple spectra) after 120 min photodegradation time at 25°C.

3.7 Quantum Yield and Band Gap Energies Measurements and Microplastic Yields

This study calculated the quantum yield to detect the number of photons emitted and absorbed. Some materials alone and high-performance light-emitting materials show a low quantum yield, which is detrimental to their practical application since lowering the photocatalysis. In our study, the quantum yield of ZIF-8/ZnO/C NCs was measured as 16%, while the quantum yields for ZIF-8, ZnO, ZIF-8/ZnO, and C were found to be low (10%, 8%, 12 and 6%), respectively (Table 1). Our study detected the maximum microplastic yields at 1 mg/l of ZIF-8/ZnO/C NCs with a quantum yield of 16%. The irradiation wavelength influences the photodegradation. Two main factors should be considered: (i) the absorption spectrum of the microplastics and (ii) how damaging the light being absorbed is. Typically, light of shorter wavelengths provides higher energy levels capable of breaking bonds, thus leading to higher photodegradation efficiencies and increased reaction rates. Nonetheless, the dependence of the wavelength on photodegradation is also related to the absorption spectrum of the irradiated compound. Sometimes, for photons to be absorbed, the spectrum of the irradiation source should overlap with the absorption spectrum of the microplastic and photocatalyst. This explains why some experience exhibited higher degrees of photodegradation when exposed to light of longer wavelengths if this matches the absorption spectrum better.

Table 1 Band gap and Quantum yield measurements for 1 mg/l ZIF-8, ZnO, ZIF-8/ZnO, ZIF-8/ZnO/C NCs and C at maximum wavelengths and microplastic yields.

Type of 1 mg/l NCs concentrations (mg/l)	Wavelengths (λ_{max}, nm)	Band Gap Energies (eV)	Quantum Yield (%)	Microplastic-PES Yields (%)	Microplastic-PVDF Yields (%)	Microplastic-PMMA Yields (%)
ZIF-8/ZnO/C NCs	345	1.34	16	99	96	93
ZIF-8	232	5.34	10	67	64	62
ZnO	420	3.89	8	62	60	58
ZIF-8/ZnO	610	2.26	12	78	76	74
C	590	4.56	6	61	56	50

The band gap energies for ZIF-8, ZnO, ZIF-8/ZnO, ZIF-8/ZnO/C and C are 5.34, 3.89, 2.26, 1.34 and 4.56 eV, respectively, at λ_{max} of 232, 420, 610, 345 and 590 nm wavelengths, respectively (Table 1). So, the composition of ZnO/C with ZIF-8 increases the light absorption amount and reduces the band gap energy. Also, it leads to a decrease in the recombination rate of induced electron-hole pairs. It is necessary to mention that the photo-absorption ability of the photocatalyst shifts to the visible light region by reduction of band gap energy.

The optimum quantum yield values observed for 1 mg/l ZIF-8/ZnO/C NCs in our study, with a band gap energy of 1.34 eV, can be attributed to its relatively lower band gap energy compared to high band gap energy ending with low microplastic yields for ZIF-8, ZnO, ZIF-8/ZnO at 1 mg/l concentrations. An optimum band gap energy generally allows a photocatalyst to absorb a broader range of the visible spectrum. Other factors such as quantum yield, charge carrier dynamics, and the specific interactions between components in the nanocomposite, can significantly influence overall photocatalytic performance. In our study, the ZIF-8/ZnO/C NCs, with their lower band gap energy of 1.34 eV, still demonstrated effective photocatalytic activity, indicating that a combination of factors including quantum yield and the efficiency of charge carrier separation and transfer, influences the photocatalytic efficiency.

The light resistance of microplastics is elevated under sunlight sources. Higher sunlight intensities cause an increase in photodegradation yields and elevated photodegradation efficiencies. Under these conditions, more electrons enter the system, and a maximal photon yield is relevant to band gap energy, as aforementıoned [32-37]. The quantum yield is a crucial point that measures the electrons during redox reactions and light variations in the microplastics. In this process, the number of photons absorbed by the photocatalyst causes a molecular response between the whole number of photons [38]. Optimum quantum efficiency is characterized by a high reaction kinetic carried out after the absorption of an electron. After the adsorption of a photon, the absorbed energy is transformed into the heat of fluorescence.

3.8 Photodegradation Mechanisms of PES, PVDF and PMMA

With appropriate comprehensive band gap metal oxide semiconductor materials, such as ZIF-8/ZnO/C NCs, distinct reactive species are produced when irradiated to sunlight. Charge separation is developed through free electrons stimulated from their valence band positions into the

conduction band when ZIF-8, ZnO, or C-related semiconductors are energized by light sources with energy more significant than their innate band gap. This stimulation enables a hole to develop in the valence band simultaneously. ROS such as hydroxyl ($OH^{\bullet}$) and superoxide ($O_2^{-\bullet}$) radicals are generated when free electrons and holes interact with H_2O, OH^-, and O_2 trapped within the semiconductor's exterior. These species trigger the micropollutant decomposition mechanism, which results in chain scission and complete mineralization into the water and carbon dioxide (CO_2). The photodegradation mechanism of ZIF-8/ZnO/C NCs was determined in Figure 10.

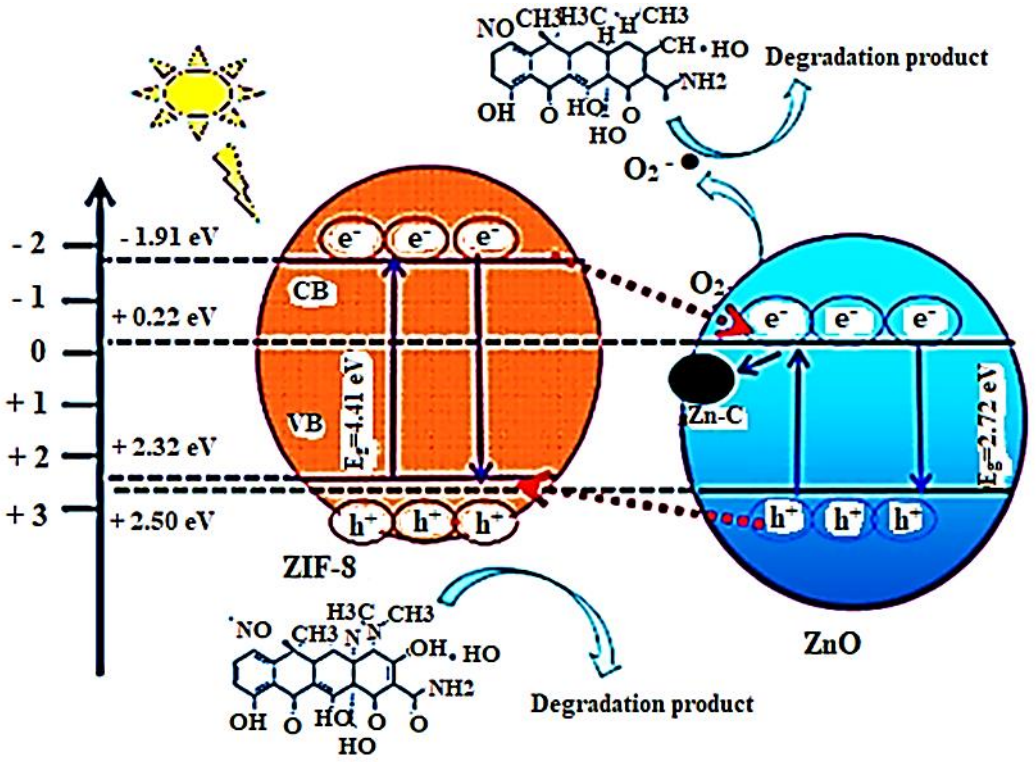

Figure 10 Photodegradation mechanism of ZIF-8/ZnO/C NCs.

It was found that broken PES residues could be successfully disintegrated by visible light-stimulated heterogeneous photocatalysis driven by ZnO-doped ZIF-8 and C. The surface area of the ZIF-8/ZnO/C NCs influenced the amount of oxidation. After extensive photocatalytic irradiation, chromophoric groups, production deformities, and weak linkages are inflection points for the oxidation reaction, resulting in the breakdown of intermolecular interactions. The reduction of electron-hole recombination is achieved by increasing visible light uptake due to photogenerated electrons into ZIF-8 from the ZnO-C anorod surfaces. The photocatalytic breakdown of PES is ensured by the production of oxygenated groups such as hydro-peroxides, peroxides, and unsaturated groups, which culminate in wrinkles, fractures, and pores with metabolites, namely hydroxymethyl, ethynyloxy radicals and acetaldehyde (Table 2). During PVDF degradation the breakdown process and intermediates reveal the formation of hydroxyl, carbonyl, and carbon-hydrogen groups with metabolites, namely 2-Propynyl, 1-hydroxy, hydroxypropyl and acetone (Table 2). During photocatalytic degradation of PMMA by-products are Butanal (Butyraldehyde) 4-Pentyn-1-olate, Hydroxypentyl, (2-ethoxyethyl) oxonium and Acetylacetonate (Table 2).

Table 2 Photodegradation metabolites of PES, PVDF and PMMA.

Ions (*m/z*)	Compounds	Molecular formula
	PES metabolites	
31	Hydroxymethyl radical	CH_3O
42	Ethynyloxy radical	C_2HO
43	Acetyl radical	CH_3CO
45	Acetaldehyde	C_2H_4O
	PVDF metabolites	
55	2-Propynyl, 1-hydroxy-	C_3H_3O
57	Hydroxypropyl	C_3H_5O
59	Acetone	C_3H_6O
	PMMA metabolites	
73	Butanal (Butyraldehyde)	$CH_3CHCOCH_3$
82	4-Pentyn-1-olate	C_5H_7O
85	Hydroxypentyl	C_5H_9O
91	(2-Ethoxyethyl) oxonium	$C_4H_{11}O_2$
99	Acetylacetonate	$C_5H_7O_2$

3.9 Factors Affecting the Photodegradation Yields of PES, PVDF and PMMA Microplastics

Possible variables that may affect photodegradation performance of PES, PVDF and PMMA are temperature, pH, time, concentrations of nanocomposites, microplastic concentration, sun ligt power based on the studies performed by Ding et al. [24], and Pasanen et al. [28] using ZIF-8 ZnO/C NCs and ZIF-8/ZnO/C NCs treating microplastics.

3.9.1 Effect of Sun Ligth Intensity on Photodegradation Yields of PES, PVDF and PMMA Microplastics

Different results were reported about microplastic photodegradation efficiencies relevant to their proportional yields depending on ligth intensity: (i) at reduced light powers the correlation is linear since the quantum efficiency is a constant. This shows that the adsorption changes with intensity; (ii) at mediate light intensities, the photodegradation yields is relevant to the square of the light intensity; (iii) at elevated light intensities, the photodegradation efficiency is not depends on the light power and remained constant.

Our study adjusted sunlight intensity between 20 W/m^2 and 120 W/m^2 at 1 mg/l ZIF-8/ZnO/C NCs concentration after 20 min. It was found that the maximum PES, PVDF, and PMMA photodegradation yields were detected at a sunlight power of 80 W/m^2 (Table 3). The PES yields were slightly higher than that PVDF and PMMA since the PES has short benzoic bounds compared to the other microplastics. A significant linear correlation was observed between sunlight intensity and microplastic yields up to a sunlight intensity of 100 W/m^2 (r^2 = 0.91, p = 0.07, F = 0.76). The ANOVA test indicated significant differences between sunlight intensity and microplastic removals for sunlight intensity >100 W/m^2 (p = 1.87, F = 9.14, d.f. = 2).

Table 3 Effect of Sunlight intensity on photodegradation yields of PES, PVDF and PMMA microplastics.

Sunlight Intensity (W/m^2)	PES Photodegradation Yield (%)	PVDF Photodegradation Yield (%)	PMMA Photodegradation Yield (%)
20	50	45	40
30	60	55	53
40	76	70	69
50	83	80	78
60	90	90	89
80	99	98	97
100	90	90	90
120	80	80	80

3.9.2 Effect of Photodegradation Time on Photodegradation Yields of PES, PVDF and PMMA Microplastics

As known, the photodegradation efficiency of organics is elevated with high durations. In some photodegradation assays, some artificial ligth sources were used to investigate microplastics' sensitivity since intensity*time relations is necessary to detect the yields of microplastics in an environment [39-42]. This analysis is necessary to estimate the duration required to attend to damage. Therefore, during the photodegradation of micropollutants, light intensity should adjusted to optimal levels to avoid inappropriate exposure times. Therefore, in this study the time was adjusted between 10 min and 100 min (Table 4). For maximum PES, PVDF and PMMA photodegradation yields, the optimum time was found to be 20 min at 1 mg/l ZIF-8/ZnO/C NCs concentration. Further, the increase in time did not affect the yields of microplastics until a photodegradation duration of 60 min. At high photodegradation times the yields of PES, PVDF and PMMA decreased. The ANOVA test indicated no significant differences between time and microplastic yields up to a photodegradation time of 40 min ($p = 0.03$, $F = 0.20$, d.f. = 2). The ANOVA test indicated significant differences between time and microplastic yields for photodegradation times >40 days ($p = 0.78$, $F = 3.19$, d.f. = 2).

Table 4 Effect of photodegradation time on photodegradation yields of PES, PVDF and PMMA microplastics.

Time (min)	PES Photodegradation Yield (%)	PVDF Photodegradation Yield (%)	PMMA Photodegradation Yield (%)
10	50	45	40
20	99	98	97
30	99	98	90
40	98	96	89
50	97	96	89
60	95	95	88

80	90	89	80
100	89	88	80

The chemical structure of the PMMA microplastic is much stronger compared to the other two microplastics therfore the yields decreased.

3.9.3 Effect of Oxygen Levels on Photodegradation Yields of PES, PVDF and PMMA Microplastics

Variations in the photodegradation efficiencies was obtained depending on the presence or absence of molecular oxygen [43-47]. Under anoxic conditions, the photocatalysis can be decreased versus the presence of a reducing or oxidizing materials. When reductive and oxidative materials are present in the photodegradation process, the types of redox materials under choosen operational conditions can define the photodegradation process. Under oxygenated conditions, the correlations between 3 D* and O_2 carried out during an energy transporting mechanism. This cause to the generation of O_2 and indicates the absence of a reductive chemical. This leads to further biodegradation of the microplastics. 3 D* may combine with O_2 with a redox process to form superoxide ions ($O_2^{-\bullet}$). An intense competition occurred when a reductive chemical was in an aerobic system. It is clear that the presence or absence of oxygen significantly affects the photodegradation yields of microplastics. The effects of oxygen levels on the photodegradation yields of PES, PVDF and PMMA microplastics are illustrated in Table 5. ANOVA test indicated no significant differences between dissolved oxygen concentration and microplastic yields up to a dissolved oxygen concentration of 5 mg/l ($p = 0.03$, $F = 0.18$, d.f. = 2). The ANOVA test indicated significant differences between dissolved oxygen and microplastic yields for dissolved oxygen concentration >4 mg/l ($p = 0.99$, $F = 3.87$, d.f. = 2).

Table 5 Effect of dissolved oxygen concentration on photodegradation yields of PES, PVDF and PMMA microplastics.

Dissolved Oxygen Concentration (mg/l)	**PES Photodegradation Yield (%)**	**PVDF Photodegradation Yield (%)**	**PMMA Photodegradation Yield (%)**
0	50	45	40
2	60	55	50
3	70	76	80
4	99	96	89
5	97	96	89
6	95	95	88
7	90	89	80
8	89	88	80

The results showed that the photodegradation yields were low at low oxygen concentrations. The maximum PES, PVDF, and PMMA yields were detected as a dissolved oxygen concentration of 4 mg/l. The most resistant microplastic was PES, while dissolved oxygen affected the PVDF and PMMA yields significantly. A lot of research exhibited that lowering oxygen dose causes a decrease in photodegradation yields. However, the photodegradation yields did not change ultimately [39-

48]. This can be attributed to some other photodegradation reactions carried out simultaneously. The level of influence of the oxygen can be attributed to the chemical properties of the microplastic. As known, oxygen can also affect the photodegradation process. In the presence of oxygen, photocatalysis is carried out quickly in oxygenated environments, resulting in the ultimate photodegradation of microplastics.

3.9.4 Effect of Temperature on Photodegradation Yields of PES, PVDF and PMMA Microplastics

Recent studies showed that temperature slightly affects the photodegradation yields of microplastics. Elevating temperature increases the fading rate, but compared to other operational conditions, temperature has a lower effect on the photodegradation of microplastics [44-46, 48]. The photodegradation efficiencies was not significantly affected by the temperature variations. Although high removal rates were detected at high temperatures, higher activation energies can be used during photodegradation. A change in temperature from 20°C up to 80°C causes a change in moisture content. As shown in Table 6, the maximum photodegradation yields for all studied microplastics were obtained at 40°C. Further, an increase in temperature did not decrease the yields significantly. In particular, at elevated temperatures, the nanocomposites have lower moisture ratios. This causes a decrease in photodegradation yields. Temperature breaks slow the aggregation of microplastics. The optical density rose with increasing temperature, ending with the decomposition of aggregates when irradiated at high temperatures; however, the optical density lowered at low temperatures, illustrating the aggregation of microplastics again. The decomposing of aggregates raised the surface area of nanocomposites after photooxidation, yielding with the raising of photodegradation. ANOVA test indicated no significant differences between temperature and microplastic yields up to a temperature of 60°C ($p = 0.02$, $F = 0.11$, d.f. = 2). The ANOVA test indicated significant differences between temperature and microplastic yields for temperature >50°C ($p = 0.97$, $F = 4.93$, d.f. = 2).

Table 6 Effect of temperature on photodegradation yields of PES, PVDF and PMMA microplastics.

Temperature (°C)	PES Photodegradation Yield (%)	PVDF Photodegradation Yield (%)	PMMA Photodegradation Yield (%)
20	50	45	40
30	60	55	50
40	99	94	93
50	99	96	89
60	97	96	89
70	95	95	88
80	88	85	80

3.9.5 Effect of Increasing ZIF-8/ZnO/C NCs Concentration on Photodegradation Yields of PES, PVDF, and PMMA Microplastics

Nanocomposite concentration affects the photodegradation yields as expected. Raising the nanocomposite dose causes elevated photodegradation yields and elevated redox reaction yield. This causes a more active surface in the nanocomposite, which is necessary for the adsorption capability of microplastics. The photodegradation yields increased with initial nanocomposite doses, and the degradation yields increased linearly with the nanocomposite dose [44, 48]. In this study, the ZIF-8/ZnO/C NCs concentration was increased from 0.1 mg/l up to 3 mg/l. Nonetheless, beyond a certain critical point, the photodegradation decreased. The maximum microplastic yields were detected at 1 mg/l ZIF-8/ZnO/C NCs dose (Table 7). An increase in turbidity of the mixture can define heterogenic photodegradation. This causes a high light scattering process and a limited light absorption of the nanocomposite. The optimal nanocatalyst dose depends on the nanocatalyst dose at the beginning. For an elevated high microplastic concentration at the beginning, an optimum dose of nanocomposite is necessary during photooxidation. Therefore, an optimal dose of nanocomposite should be present to provide an effective photooxidation process. ANOVA test indicated that there were no significant differences between ZIF-8/ZnO/C NCs concentration and microplastic yields up to a ZIF-8/ZnO/C NCs concentration of 1.2 mg/l ($p = 0.03$, $F = 0.10$, d.f. = 2). ANOVA test indicated that there were significant differences between ZIF-8/ZnO/C NCs concentration and microplastic yields for ZIF-8/ZnO/C NCs concentration >1.0 mg/l ($p = 0.99$, $F = 4.74$, d.f. = 2).

Table 7 Effect of increasing ZIF-8/ZnO/C NCs concentration on photodegradation yields of PES, PVDF, and PMMA microplastics.

ZIF-8/ZnO/C NCs Concentration (mg/l)	PES Photodegradation Yield (%)	PVDF Photodegradation Yield (%)	PMMA Photodegradation Yield (%)
0.1	50	45	40
0.5	60	55	50
0.7	80	78	69
1.0	99	96	90
1.2	97	96	89
1.5	95	95	88
3.0	88	85	80

A nanocomposite improves the photooxidation yield by producing reactive radical species on its surface after irradiation with a light of energy higher than the bandgap of the catalyst. During photooxidation, electrons are emitted from the conduction band, which provides positive holes (h^+) in the valence band of the nanocomposite. Oxygen and water molecules are transformed into the reactive $O_2^{-\bullet}$ and $OH^\bullet$ radicals, respectively. This leads to reacting continuously with adsorbed microplastics [45, 46]. The heterostructure of ZIF-8/ZnO/C NCs with high synergistic effect electronic interaction exhibited higher photocatalytic activity than pure ZnO, ZIF-8, or C.

3.9.6 Effect of Increasing Microplastic Concentration on Photodegradation Yields of PES, PVDF and PMMA Microplastics

Photooxidation is significantly correlated with the microplastic dose in the liquid mixtures. At elevated microplastic doses, the optimum size of the nanocomposite aggregates decreased the surface area accessible to environmental factors. Therefore, at elevated microplastic concentration, the aggregation mechanism rises, Causing lower photodegradation efficiencies. Increased microplastic concentrations increase the absorption of microplastics on the surface of the nanocomposite. This caused decreased interactions between the microplastic and nanocomposite and low photodegradation efficiencies were detected. In heterogeneous photocatalytic systems like our study, the initial microplastic concentration has a pronounced impact on photodegradation yields. Table 8 shows the photodegradation yields of microplastics at concentrations between 50 and 1200 mg/l. The maximum PES, PVDF and PMMA yields were detected at 1000 mg/l microplastic concentration while the further increase of concentrations significantly decreased the yields (Table 8). ANOVA test showed no significant differences between microplastic concentration and microplastic yields up to a microplastic concentration of 1100 mg/l ($p = 0.05$, $F = 0.08$, d.f. = 2). The ANOVA test indicated significant differences between microplastic concentration and microplastic yields for a microplastic concentration >1000 mg/l ($p = 0.97$, $F = 5.66$, d.f. = 2).

Table 8 Effect of increasing microplastic concentration on photodegradation yields of PES, PVDF and PMMA microplastics.

Microplastic Concentration (mg/l)	PES Photodegradation Yield (%)	PVDF Photodegradation Yield (%)	PMMA Photodegradation Yield (%)
50	99	98	96
100	99	98	96
200	99	98	96
300	99	98	96
400	99	98	96
500	99	98	96
600	99	98	96
700	99	98	96
800	99	98	96
900	99	98	96
1000	99	98	96
1100	78	67	60
1200	70	65	50

The production of $OH^{\bullet}$ radicals on the photocatalytic surface was covered at an elevated microplastic dose. Lower photons attained the catalyst surface since the absorbance by the microplastics decreased. This causes a lowering of reactive radical production by the nanocomposite, resulting in lower photooxidation efficiencies [42].

3.9.7 Effect of Increasing pH on Photodegradation Yields of PES, PVDF, and PMMA Microplastics

Photodegradation can be affected significantly by the pH. Some activated groups can be protonated or deprotonated under acidic or alkaline pH. This causes the lowering or increasing of photolysis efficiencies. This study adjusted the pH to acidic, neutral, and alkaline levels to detect the optimal pH conditions for maximal PES, PVDF, and PMMA microplastic photodegradation yields (Table 9). ANOVA test showed no significant differences between pH and microplastic yields ($p = 0.03$, $F = 0.05$, d.f. = 2). A significant linear correlation between pH and microplastic yield was detected ($r = 0.93$, $F = 0.05$, d.f. = 2).

Table 9 Effect of increasing pH on photodegradation yields of PES, PVDF, and PMMA microplastics.

pH	PES Photodegradation Yield (%)	PVDF Photodegradation Yield (%)	PMMA Photodegradation Yield (%)
5	50	45	40
7	65	58	57
10	99	98	96

The pH impact on the photodegradation of micropollutants is relevant to their chemical structure and pKa value. The charged electrons in nanocomposite are more prone to a photodegradation reaction. Therefore, the photooxidation of microplastics elevated at pH values higher than their pKa, where these molecules are negatively charged [41, 45, 46]. The photofading efficiency of the microplastics is also elevated at pH values smaller than its pKa, where the molecule presents in cation form [42]. It is also important to note that the pH variations cause protonation or deprotonation of the microplastics. In heterogeneous photocatalytic systems, photodegradation is indirectly affected by the pH, the type of solid nanocomposite, and the microplastic metabolites. pH impacts the electrostatic relationships between the substrates on the surface of the photocatalyst and the microplastics. As a result, the adsorption capacity of the catalyst can be varied. Therefore, at a lower pH, the protonation of the nanocomposite occurred. This causes a positively charged surface, whereas a negatively charged surface will be formed at elevated pH levels. Our study found the maximum microplastic photodegradation rates at pH = 10.0 (Table 9). In environmental ecosystems such as lakes, rivers and bays with pH ranging between 7.8 and 8.9, the PES, PVDF and PMMA microplastics yields were detected as 89%, 79% and 70%, respectively (data not shown).

Since no more studies were detected investigating the PES, PVDF and PMMA microplastics photoremoval via ZIF-8 MOF containing ZnO our efficiencies were compared with only two studies: Ding et al. [24] investigated the ptotocatalytic yields of PES and PVDF using 6 mg/l ZIF-8/ZnO/C nanocomposite. Low PES and PVDF yields (67-72%) at long photodegradation times (130 min), and high UV light power (290 W/m^2) were detected and compared to our data. In our study 98-99% PES, PVDF and PMMA yields was detected at short times, as low as 20 min at a low sun light power of 80 W/m^2. The dose of ZIF-8/ZnO/C nanocomposite used in our study was low (1.3 mg/l) showing the economic aspect of our study. Pasanen et al. [28] prepared a ZIF-8 magnetic porous nanocomposite (nano-Fe@ZIF-8) to remove the PMMA and PES microplastics and plastic-derived endocrine disruptors. 78% and 85% PMMA and PES yields were detected after 190 min at acidic pH at 34 mg/l

ZIF-8 MOF containing ZnO concentration at a UV power of 120 W/m^2 for maximum initial 6 and 8 mg/l PMMA and PES concentration, respectively. In our study, the maximum PES and PMMA yields were 98% and 97% after 20 min at sunlight of 89 W/m^2 at high PES and PMMA concentrations of 1000 mg/l. Our study detected high PES and PMMA yields at short photodegradation times at high microplastic loadings with low ZIF-8/ZnO/C NCs nanocomposite concentrations.

3.9.8 Future Scope of Photodegradation of PES, PVDF and PMMA Microplastics

In this study, although, the physicochemival properties of the ZIF-8, ZnO, ZIF-8/ZnO and ZIF-8/ZnO/C NCs were investigated, the effects of operational conditions were also investigated only for ZIF-8/ZnO/C NCs. Moreover, it is impossible to accurately predict the treatment of the microplastics as mentioned above distributed in wastewater effluents. The toxicity of the metabolites of PES, PVDF, and PMMA microplastics during photodegradation while being emitted to the environmental ecosystem should be investigated. The significant part of the research focuses on water contamination, with just a few studies examining pollution in atmospheric and terrestrial settings. The recovery of the ZIF-8/ZnO/C NCs studies should be performed to determine the cost-effective situation of the nanocomposite. Large full-scale applications, such as in the soil and nearshore marine systems, should be investigated for possible photodegradation mechanisms of PES, PVDF and PMMA microplastics. Removing these microplastics from water, soil, and sediment is possible using ZIF-8/ZnO/C NCs.

4. Conclusions

This study produced a MOF nanocomposite, namely ZIF-8/ZnO/C NCs, under laboratory conditions to photodegrade the PES, PVDF and PMMA microplastics. The XRD analysis showed the formation of ZIF-8/ZnO/C NCs, while the FTIR analysis indicated the presence of ZnO, C and ZIF-8. For maximum PES (99%), PVDF (98%) and PMMA (96%) microplastics photodegradation yield the operational and environmental conditions should be as follows: 1 mg/l ZIF-8/ZnO/C NCs concentration, 1000 mg/l microplastic concentration, pH = 10.0, temperature = 40°C, sunlight intensity = 80 W/m^2, dissolved oxygen concentration = 4 mg/l and photodegradation time = 20 min. When microplastic photodegradation occurs, several operational and environmental conditions should be considered before evaluating the microplastics' reaction mechanism. These conditions should contain the substrate's chemical structure, the nanocomposite's complexity and its susceptibility versus photocatalysis, and the interactions with the operational and environmental factors.

More research is needed to investigate the long-term stability of ZIF-8/ZnO/C NCs in aqueous environments and develop efficient regeneration methods for their repeated use. This can include examining the effects of water chemistry and exploring regeneration methods such as heating or washing to ensure the long-term effectiveness of ZIF-8/ZnO/C NCs during microplastic photodegradation. Climate change and long periods of drought affect clean water supplies, while contaminants such as microplastics can pollute clean water sources and cause disease outbreaks. Utilizing ZIF-8/ZnO/C NCs in polluted water can help supply clean water for the increasing population.

More research is needed to explore the practical implementation of ZIF-8/ZnO/C nanocomposites for microplastic removal on a larger scale, including their cost-effectiveness and

scalability. Nonetheless, ZIF-8/ZnO/C represents a promising avenue for developing innovative solutions to address the ongoing issue of environmental micropollutant pollution.

Author Contributions

Post-Dr. Rukiye Öztekin: Conceptualization, methodology, writing – original draft, formal analysis, writing – review and editing. Prof. Dr. Delia Teresa Sponza: Conceptualization, methodology, writing – original draft, formal analysis, writing – review and editing, and also, the final control of draft. All authors read and approved the published version of the article.

Competing Interests

The authors have declared that no competing interests exist.

References

1. Dzihninafira H, Razi F. Microplastic removal in Krueng Aceh river water using ultrafiltration membrane from polyethersulfone polymer (PES). Indones J Chem Anal. 2023; 6: 151-163.
2. Ding Z, Li W, Chen Z, Wang L, Huang S, Evrendilek F, et al. Microplastics as emerging contaminants in textile dyeing sludge: Their impacts on co-combustion/pyrolysis products, residual metals, and temperature dependency of emissions. J Hazard Mater. 2024; 466: 133465.
3. Liu J, Jia D, Xu W, Chen Z, Evrendilek F, Cao H, et al. Catalytic pyrolysis of $FeAlO_x$ and medical plastic waste: Kinetic, slag conversion, and gas emission patterns. J Environ Chem Eng. 2024; 12: 112605.
4. Das TK, Basak S, Ganguly S. 2D nanomaterial for microplastic removal: A critical review. Chem Eng J. 2024; 492: 152451.
5. Das TK, Jesionek M, Çelik Y, Poater A. Catalytic polymer nanocomposites for environmental remediation of wastewater. Sci Total Environ. 2023; 901: 165772.
6. Das TK. Polymer composite sensors: Environmental aspects, health hazards, and degradation. In: Polymeric nanocomposite materials for sensor applications. Thorston, UK: Woodhead Publishing; 2023. pp. 521-540.
7. Bhawal P, Das TK, Ganguly S, Mondal S, Ravindren R, Das NC. Fabrication of light weight mechanically robust short carbon fiber/ethylene methyl acrylate polymeric nanocomposite for effective electromagnetic interference shielding. J Polym Sci Appl. 2017; 1: 1000107.
8. Honarmandrad Z, Kaykhaii M, Gębicki J. Microplastics removal from aqueous environment by metal organic frameworks. BMC Chem. 2023; 17: 122.
9. Abdeljaoued A, Ruiz BL, Tecle YE, Langner M, Bonakdar N, Bleyer G, et al. Efficient removal of nanoplastics from industrial wastewater through synergetic electrophoretic deposition and particle-stabilized foam formation. Nat Commun. 2024; 15: 5437.
10. Nikhar S, Kumar P, Chakraborty M. A review on microplastics degradation with MOF: Mechanism and action. Next Nanotechnol. 2024; 5: 100060.
11. Nikiema J, Asiedu Z. A review of the cost and effectiveness of solutions to address plastic pollution. Environ Sci Pollut Res. 2022; 29: 24547-24573.

12. Zhao R, Nie Y, Liu J, Wang Y, Li N, Cheng Q, et al. New insight into ZnO@ZIFs composite: An efficient photocatalyst with boosted light response ability and stability for CO_2 reduction. Environ Sci Pollut Res. 2023; 30: 82672-82685.
13. Liu S, Wang J, Yu J. ZIF-8 derived bimodal carbon modified ZnO photocatalysts with enhanced photocatalytic CO_2 reduction performance. RSC Adv. 2016; 6: 59998-60006.
14. Liu N, Shang S, Shi D, Cheng Q, Pan Z. Construction of hollow ZnO/Mn-ZIF-67 heterojunction photocatalysts: Enhanced photocatalytic performance and mechanistic insight. New J Chem. 2021; 45: 2285-2294.
15. Liu Y, Deng L, Sheng J, Tang F, Zeng K, Wang L, et al. Photostable core-shell CdS/ZIF-8 composite for enhanced photocatalytic reduction of CO_2. Appl Surf Sci. 2019; 498: 143899.
16. Hussain MZ, Schneemann A, Fischer RA, Zhu Y, Xia Y. MOF derived porous ZnO/C nanocomposites for efficient dye photodegradation. ACS Appl Energy Mater. 2018; 1: 4695-4707.
17. Ranjithkumar R, Arasi SE, Sudhahar S, Nallamuthu N, Devendran P, Lakshmanan P, et al. Enhanced electrochemical studies of ZnO/CNT nanocomposite for supercapacitor devices. Physica B Condens Matter. 2019; 568: 51-59.
18. Venugopal N, Yang BC, Ko T. ZnO/CNT nanocomposite electrode for aqueous electrochemical supercapacitor. Mater Res Innov. 2012; 16: 96-100.
19. Wang W, Jiao S, Cao J, Naguib HE. Zinc oxide/carbon nanotube nanocomposite for high-performance flexible supercapacitor with sensing ability. Electrochim Acta. 2020; 350: 136353.
20. De B, Banerjee S, Verma KD, Pal T, Manna PK, Kar KK. Carbon nanotube as electrode materials for supercapacitors. In: Handbook of nanocomposite supercapacitor materials II: Performance. Cham: Springer; 2020. pp. 229-243.
21. Xia H, Zhang J, Yang Z, Guo S, Guo S, Xu Q. 2D MOF nanoflake-assembled spherical microstructures for enhanced supercapacitor and electrocatalysis performances. Nanomicro Lett. 2017; 9: 43.
22. Liu B, Shioyama H, Jiang H, Zhang X, Xu Q. Metal-organic framework (MOF) as a template for syntheses of nanoporous carbons as electrode materials for supercapacitor. Carbon. 2010; 48: 456-463.
23. Otun KO, Liu X, Hildebrandt D. Metal-organic framework (MOF)-derived catalysts for Fischer-Tropsch synthesis: Recent progress and future perspectives. J Energy Chem. 2020; 51: 230-245.
24. Ding A, Tai W, Li Q, Liu X, Li H, Yao C. Using ZIF-8 to synthesize ZnO/C composite with enhanced photocatalytic property. J Iran Chem Soc. 2023; 20: 2517-2525.
25. He L, Li L, Wang T, Gao H, Li G, Wu X, et al. Fabrication of Au/ZnO nanoparticles derived from ZIF-8 with visible light photocatalytic hydrogen production and degradation dye activities. Dalton Trans. 2014; 43: 16981-16985.
26. Abdollahi B, Najafidoust A, Asl EA, Sillanpaa M. Fabrication of ZiF-8 metal organic framework (MOFs)-based CuO-ZnO photocatalyst with enhanced solar-light-driven property for degradation of organic dyes. Arab J Chem. 2021; 14: 103444.
27. Chao S, Li X, Li Y, Wang Y, Wang C. Preparation of polydopamine-modified zeolitic imidazolate framework-8 functionalized electrospun fibers for efficient removal of tetracycline. J Colloid Interface Sci. 2019; 552: 506-516.

28. Pasanen F, Fuller RO, Maya F. Fast and simultaneous removal of microplastics and plastic-derived endocrine disruptors using a magnetic ZIF-8 nanocomposite. Chem Eng J. 2023; 455: 140405.
29. Fan G, Zheng X, Luo J, Peng H, Lin H, Bao M, et al. Rapid synthesis of Ag/AgCl@ZIF-8 as a highly efficient photocatalyst for degradation of acetaminophen under visible light. Chem Eng J. 2018; 351: 782-790.
30. IUPAC. Compendium of chemical terminology. 2nd ed. Zurich, Switzerland: International Union of Pure and Applied Chemistry; 1997. Available from: https://goldbook.iupac.org/terms/view/Q04991.
31. Dong H, Wang X, Niu X, Zeng J, Zhou Y, Suona Z, et al. Overview of analytical methods for the determination of microplastics: Current status and trends. Trends Analyt Chem. 2023; 167: 117261.
32. Samadi M, Shivaee HA, Zanetti M, Pourjavadi A, Moshfegh A. Visible light photocatalytic activity of novel MWCNT-doped ZnO electrospun nanofibers. J Mol Catal A Chem. 2012; 359: 42-48.
33. Bindumadhavan K, Srivastava SK, Mahanty S. MoS_2-MWCNT hybrids as a superior anode in lithium-ion batteries. Chem Commun. 2013; 49: 1823-1825.
34. Li WC, Mak CL, Kan CW, Hui CY. Enhancing the capacitive performance of a textile-based CNT supercapacitor. RSC Adv. 2014; 4: 64890-64900.
35. Sarkar A, Chakraborty AK, Bera S, Krishnamurthy S. Novel hydrothermal synthesis of CoS_2/MWCNT nanohybrid electrode for supercapacitor: A systematic investigation on the influence of MWCNT. J Phys Chem C. 2018; 122: 18237-18246.
36. Sasirekha C, Arumugam S, Muralidharan G. Green synthesis of ZnO/carbon (ZnO/C) as an electrode material for symmetric supercapacitor devices. Appl Surf Sci. 2018; 449: 521-527.
37. Gao Q, Xu J, Bu XH. Recent advances about metal-organic frameworks in the removal of pollutants from wastewater. Coord Chem Rev. 2019; 378: 17-31.
38. Li X, Wang Z, Qiu Y, Pan Q, Hu P. 3D graphene/ZnO nanorods composite networks as supercapacitor electrodes. J Alloys Compd. 2015; 620: 31-37.
39. Azqhandi MH, Rajabi FH, Keramatifarhodbonab M. Synthesis of Cd doped ZnO/CNT nanocomposite by using microwave method: Photocatalytic behavior, adsorption and kinetic study. Results Phys. 2017; 7: 1106-1114.
40. Chaudhary D, Singh S, Vankar VD, Khare N. ZnO nanoparticles decorated multi-walled carbon nanotubes for enhanced photocatalytic and photoelectrochemical water splitting. J Photochem Photobiol A Chem. 2018; 351: 154-161.
41. Hojati T, Ebrahimi M, Afzalzadeh R. Highly sensitive CO sensor based on ZnO/MWCNT nano sheet network grown via hydrothermal method. Mater Chem Phys. 2018; 207: 50-57.
42. Bhagwan J, Hussain SK, Krishna BV, Yu JS. Facile synthesis of $MnMoO_4$@MWCNT and their electrochemical performance in aqueous asymmetric supercapacitor. J Alloys Compd. 2021; 856: 157874.
43. Saravanakumar B, Purushothaman KK, Muralidharan G. V_2O_5/functionalized MWCNT hybrid nanocomposite: The fabrication and its enhanced supercapacitive performance. RSC Adv. 2014; 4: 37437-37445.
44. Wu F, Wang X, Hu S, Hao C, Gao H, Zhou S. Solid-state preparation of CuO/ZnO nanocomposites for functional supercapacitor electrodes and photocatalysts with enhanced photocatalytic properties. Int J Hydrogen Energy. 2017; 42: 30098-30108.

45. Lee KS, Park CW, Kim JD. Synthesis of ZnO/activated carbon with high surface area for supercapacitor electrodes. Colloids Surf A Physicochem Eng Asp. 2018; 555: 482-490.
46. Subramani K, Sathish M. Facile synthesis of ZnO nanoflowers/reduced graphene oxide nanocomposite using zinc hexacyanoferrate for supercapacitor applications. Mater Lett. 2019; 236: 424-427.
47. Zhu C, He Y, Liu Y, Kazantseva N, Saha P, Cheng Q. ZnO@MOF@PANI core-shell nanoarrays on carbon cloth for high-performance supercapacitor electrodes. J Energy Chem. 2019; 35: 124-131.
48. Dhillon S, Kant R. Theory for electrochemical impedance spectroscopy of heterogeneous electrode with distributed capacitance and charge transfer resistance. J Chem Sci. 2017; 129: 1277-1292.